CONF-8805141--2

DE88 011833

CRACK ARREST BEHAVIOR OF REACTOR PRESSURE VESSEL STEELS AT HIGH TEMPERATURES

C. E. Pugh, D. J. Naus, and B. R. Bass
Oak Ridge National Laboratory (ORNL)
Oak Ridge, Tennessee 37831

CRACK ARREST BEHAVIOR OF REACTOR PRESSURE VESSEL STEELS AT HIGH TEMPERATURES*

C. E. Pugh, D. J. Naus, and B. R. Bass
Oak Ridge National Laboratory (ORNL)
Oak Ridge, Tennessee 37831

ABSTRACT

The Heavy-Section Steel Technology Program at the Oak Ridge National Laboratory under the sponsorship of the U.S. Nuclear Regulatory Commission is conducting experimental and analytical studies to improve the understanding of conditions that govern the initiation, rapid propagation, arrest and ductile tearing of cracks in reactor pressure vessel (RPV) steels. In support of this objective, large-scale wide-plate experiments are performed to generate crack-arrest toughness data for RPV steels at temperatures approaching and above the onset of Charpy upper-shelf behavior. Analytical studies are addressing the role of dynamics and nonlinear rate-dependent (i.e., viscoplastic) effects in the interpretation of crack run-arrest events in these ductile materials. A summary of the wide-plate tests performed to date is presented, including details of test procedures, test data, and results of analyses performed to date. The importance of incorporating viscoplastic effects into dynamic analyses of crack run-arrest events in these strain-rate sensitive steels is examined through applications of selected proposed viscoplastic constitutive equations and fracture parameters to the interpretation of data from the wide-plate tests. The crack-arrest data are compared with those from small ASTM-type specimens and other large structural tests.

1. INTRODUCTION

The Oak Ridge National Laboratory (ORNL) is continuing under the Heavy-Section Steel Technology (HSST) Program to improve the understanding of conditions that govern the initiation, rapid propagation, arrest, and ductile tearing of cracks in reactor pressure vessel (RPV) steels. In pressurized-thermal-shock (PTS) scenarios, inner surface cracks in a RPV have the greatest propensity to propagate because they are located in the region of highest thermal stress, lowest temperature and greatest irradiation damage. If such a crack begins to propagate radially through the vessel wall, it will extend into a region of higher fracture toughness due to the higher temperatures and less irradiation damage. Assessment of the integrity of a RPV under such a postulated crack run-arrest scenario requires prediction of the arrest location,

---

*Research sponsored by the Office of Nuclear Regulatory Research, U.S. Nuclear Regulatory Commission under Interagency Agreements 0551-0551-A1 and 0552-0552-A1 with the U.S. Department of Energy under Contract DE-AC05-84OR21400 with Martin Marietta Energy Systems, Inc.

potential reinitiation, stable or unstable ductile crack growth, and structural instability of the remaining vessel wall ligament.

The HSST Program is sponsored by the U.S. Nuclear Regulatory Commission (NRC) and is conducting experimental and analytical studies aimed at providing this better understanding as a part of their overall pressure vessel research program. Experimentally, large-scale tests are being carried out to generate crack-arrest toughness data at temperatures approaching and above the onset of Charpy upper-shelf behavior. These tests involve large thermally-shocked cylinders, pressurized-thermally-shocked vessels, and wide-plate specimens. The highest number of data points are being generated in these studies by the wide-plate tests which are conducted at the National Bureau of Standards. Objectives of these tests are to: (1) extend the existing K_{Ia} data bases for selected materials to values above the limit in the ASME Code, (2) clearly establish that cleavage crack propagation exhibits arrest prior to fracture-mode conversion, (3) provide data to improve and validate elastic and viscoplastic dynamic fracture-mechanics models, and (4) develop improved experimental dynamic fracture methods. Thirteen wide-plate experiments have been performed to date using two steels. The first specimens are designated as series WP-1 and were from a A533 grade B, class 1 steel plate that has good properties including a high (~160 J) Charpy upper-shelf energy. The second material, a specially heat-treated 2 1/4 Cr-1 Mo steel, has a low (~50 J) Charpy upper-shelf energy and the specimens are designated as series WP-2. The high-temperature arrest conditions are obtained by driving a crack from a chilled side of a large non-isothermal single-edge-notched plate specimen (1 × 1 × 0.10 m) into a warmer, heated part of the plate.

Analytically, the HSST crack-arrest studies are including dynamic fracture modeling and the development of computational analysis methods which incorporate nonlinear and strain-rate dependent (i.e., viscoplastic) effects for use in interpreting crack run-arrest events in these ductile materials. In a portion of these studies, various viscoplastic constitutive models and several proposed nonlinear fracture criteria have been installed in two HSST-developed finite element computer programs. The capabilities of these nonlinear techniques are being compared and evaluated, in part, through applications to the wide-plate tests.

The following sections provide a summary of the two series of wide-plate crack-arrest tests, including details of the test procedures, data from the tests completed, and the result of analyses performed to date. The results from the wide-plate tests are compared with those from other large-specimen tests. This is followed by a discussion of the importance of incorporating viscoplastic effects into dynamic fracture analyses of crack run-arrest events in these strain-rate sensitive ductile steels. Finally, computed inelastic fracture parameters are compared in detail with elastodynamic analysis results for one of the wide-plate tests.

2. MATERIAL PROPERTIES

2.1 WP-1 Test Series (A533B Material)

The initial series of HSST wide-plate crack-arrest specimens is taken from the central portion of the 18.73-cm-thick plate (designated as HSST plate 13A) of A533 grade B class 1 steel that is in a quenched and tempered condition. Properties of the plate include Young's modulus (E) = 206.9 GPa, Poisson's ratio (ν) = 0.3, coefficient of thermal expansion (α) = 11×10^{-6}/°C, and density (ρ) = 7850 kg/m^3. The temperature-dependent yield stress for the material is given by

$$\sigma_y = 374.87 + 59.89e^{-0.00793T} \tag{1}$$

where σ_y and T have units in megapascals and degrees Celcius, respectively. Temperature-dependent fracture-toughness relations for initiation and arrest, based on small-specimen data, are given by

$$K_{Ic} = 51.28 + 51.90e^{0.036(T - RT_{NDT})} \tag{2}$$

$$K_{Ia} = 49.96 + 16.88e^{0.029(T - RT_{NDT})} \tag{3}$$

with units for K and T being MPa$\cdot\sqrt{m}$ and °C, respectively. Drop-weight and Charpy V-notch test data indicate that RT_{NDT} = -23°C, and Charpy upper-shelf energy is 160 J with its onset occurring at 55°C, as depicted in Fig. 1.

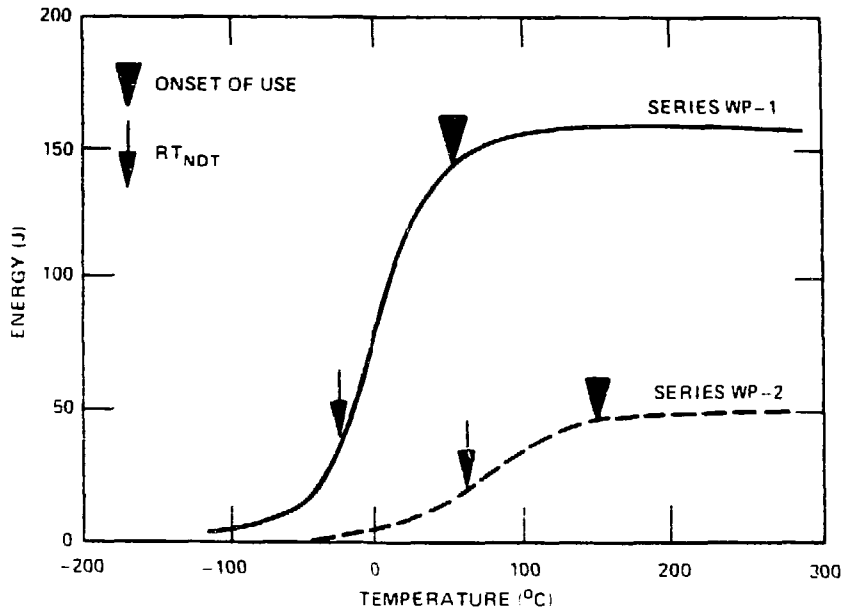

Fig. 1. Charpy V-notch energy versus temperature for materials used in the first two series of wide-plate crack-arrest tests.

Analytical studies have used a dynamic fracture toughness relation in the following form:

$$K_{ID} = K_{Ia} + A(T)\,\dot{a}^2 \quad , \tag{4}$$

where K_{Ia} is given by Eq. (3) and

$$A(T) = [329.7 + 16.25\,(T - RT_{NDT})] \times 10^{-6} \quad , \tag{5}$$

or

$$A(T) = [121.71 + 1.296\,(T - RT_{NDT})] \times 10^{-6} \quad , \tag{6}$$

if $(T - RT_{NDT})$ is greater or less than -13.9°C, respectively. Units for K_{ID}, A, $\dot{a}$, and T are megapascals times root meters, megapascals times square seconds times meters to the -3/2, meters per second, and degrees Celcius, respectively. The form of the K_{ID} expression in Eq. (4) and relations for A(T) [Eqs. (5) and (6)] are derived from Ref. 1 by estimating that RT_{NDT} = -6.1°C for the material used in that study.

2.2 WP-2 Test Series (Low Upper-Shelf Material)

The second (WP-2) series of wide-plate crack-arrest specimens is taken from the left-hand portion of a 15.88-cm thick plate of 2 1/4 Cr-1 Mo steel. The material, which was supplied by Babcock and Wilcox, was heat treated in order to obtain a Charpy upper-shelf energy equal to or less than 68 Joules (50 ft-lb). All characterization testing of this material has not been completed yet, so detailed property data are not available.

Based on a limited number of tests, the tentative drop-weight nil-ductility temperature for the material is > 60°C, and the Charpy upper-shelf energy is about 50 J with its onset occurring at about 150°C (Fig. 1). The yield strength (σ_y) and ultimate strength (σ_u) of the material, for use in tensile instability calculations, are taken to be 320 MPa and 500 MPa, respectively. Preliminary temperature-dependent fracture-toughness relations for initiation and arrest, based on results of a limited number of compact-type-specimen tests, have been developed and used in planning the WP-2 series tests.

$$K_{Ic} = 39.53 + 93.47e^{0.036(T - DW_{NDT})} \tag{7}$$

$$K_{Ia} = 22.31 + 62.69e^{0.0177(T - DW_{NDT})} \quad , \tag{8}$$

where the units of K_I and T are MPa·$\sqrt{m}$ and °C, respectively, and the material DW_{NDT} = 60°C. An RT_{NDT} could not be established by ASME criteria because the Charpy upper shelf energy was below the 68 J level.

3. SPECIMEN PREPARATION, INSTRUMENTATION AND TESTING PROCEDURE

The 1 by 1 by 0.1 m specimens (1 by 1 by 0.15 m specimens for WP-1.7, WP-2.1 and WP-2.3), shown schematically in Fig. 2, were machined and precracked by ORNL. The precracking was done by hydrogen charging an electron-beam (EB) weld located at the base of a premachined notch in the plate. The total crack length, notch depth plus EB weld, for each specimen was nominally 0.2 m (a/W ~ 0.2), and the flaw was oriented perpendicular to the rolling direction. Each side of the specimens was side grooved to a depth equal to 12.5% of the plate thickness. Starting with the third specimen in test series WP-1 (WP-1.3), the crack front of each specimen, with the exception of WP-2.3, was machined into a truncated chevron configuration to reduce the tensile load required to achieve crack initiation. Upon completion of the machining operations, each specimen was shipped to NBS where it was welded to pull plates nominally

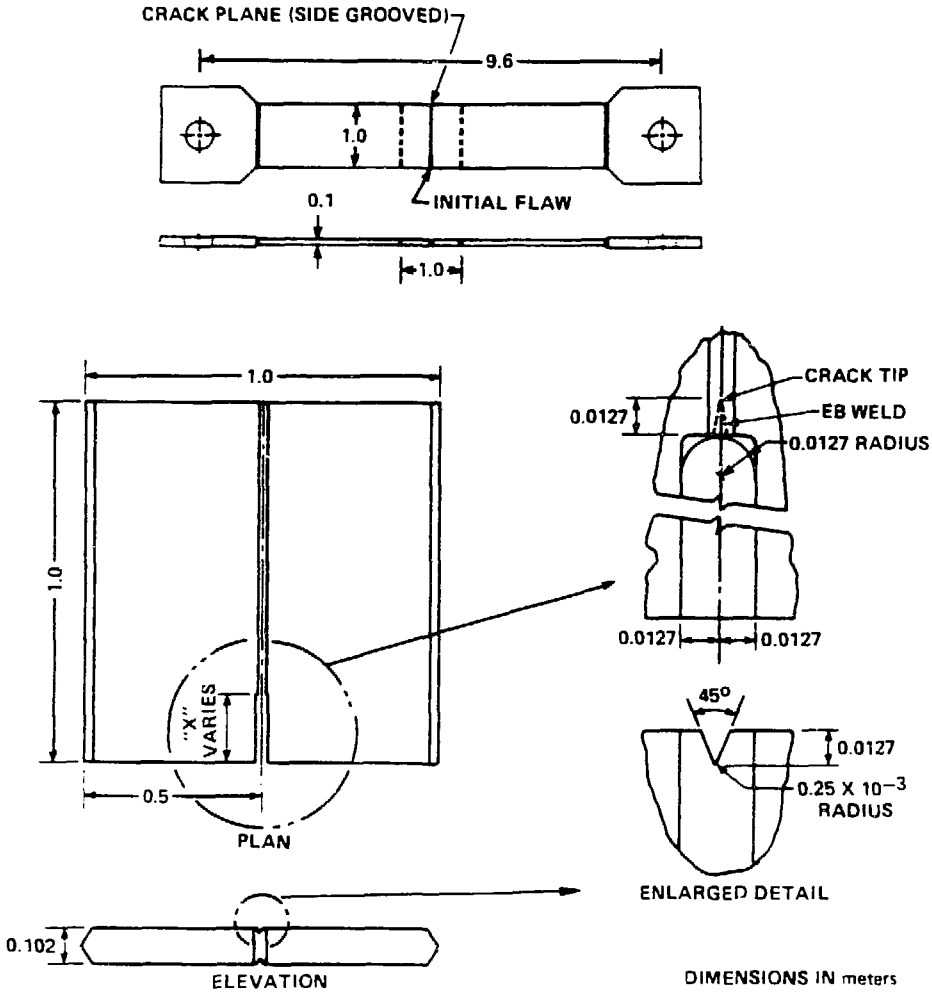

Fig. 2. Schematic of HSST wide-plate crack-arrest specimen.

having the same cross-section geometry as the specimen. A specimen pin-to-pin length of approximately 9.6 m was selected to minimize stress wave effects. Tables 1 and 2 present dimensions for each specimen in the WP-1 and WP-2 test series, respectively, which has been tested to date.

Up to a total of 25 strain gages have been placed on the specimens to provide dynamic strain-field measurements for determining crack velocity and assessing boundary conditions. As an example, the strain gage locations utilized for test WP-1.6 are shown in Fig. 3. The strain signals

Table 1. WP-1 series test specimen dimensions

Dimension	Symbol[a]	Dimension (mm)						
		Specimen designation						
		WP-1.1	WP-1.2	WP-1.3	WP-1.4	WP-1.5	WP-1.6	WP-1.7
Initial crack length	a_o	196.9	199	197	207.5	200	200	202
Thickness	B	101	101.8	99.5	99.6	101.7	101.8	152.4
Notched thickness	B_N	76.3	77.5	75.4	76.9	76.4	75.5	114.3
Chevron thickness (thickness at a_o)	B_C	NA[b]	NA[b]	47.5	33.8	41.2	40.0	61.0
Width	W	997	998	1000	1000	1000	1000	1000

[a]See Fig. 2.

[b]Not applicable.

Table 2. WP-2 series test specimen dimensions

Dimension	Symbol[a]	Dimension (mm)			
		Specimen designation			
		WP-2.4	WP-2.1	WP-2.5	WP-2.3
Initial crack length	a_o	203	202.6	199	200
Thickness	B	101.7	152.3	101.6	152.4
Notch thickness	B_N	76.3	113.9	76.2	113.8
Chevron thickness (thickness at a_o)	B_C	40.5	61.5	40.7	c
Width	W	1000	1000	999	1000
Pop-in crack length	a'_o	251	NA[b]	264	NA[b]
Chevron thickness (thickness at a'_o)	B'_C	75.5	NA[b]	NA[b]	c

[a]See Fig. 2.

[b]Not applicable because either a pop-in did not occur (WP-2.1 and WP-2.3) or the crack length after pop-in (a'_o) was past the region of the plate where the crack front had been chevroned (WP-2.5).

[c]Specimen non-chevroned.

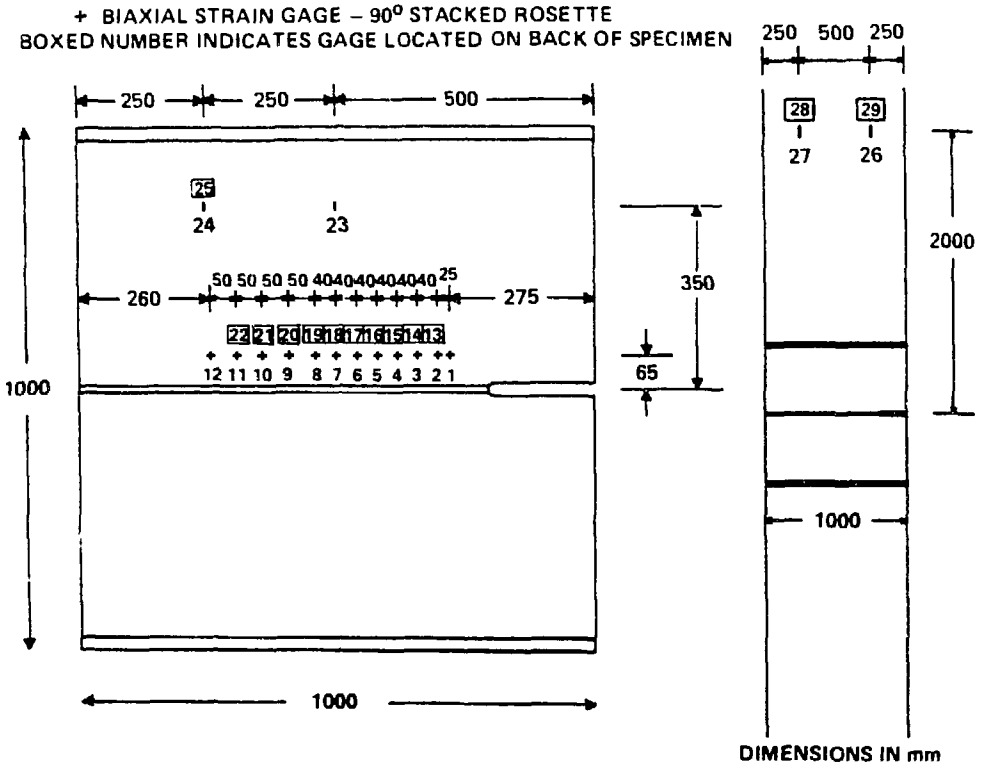

Fig. 3. Strain gage locations for a typical HSST wide-plate crack-arrest specimen.

were recorded either by a transient digital oscilloscope or a combination of oscilloscopes and a multichannel, wide band, frequency modulated, magnetic tape recorder. Up to 33 thermocouples were positioned on each specimen and sequentially monitored to insure that the desired temperature distribution was achieved throughout the plate assembly. Additional instrumentation included two capacitance-based crack-opening-displacement (COD) gages mounted on the front and back surface of the plate at an a/W that varied from 0.120 to 0.175 from test to test. More detailed information on the instrumentation systems can be obtained from Ref. [2].

In each wide-plate test, a temperature gradient was imposed across the plate by LN_2 cooling of the notched edge while heating the other edge. Final calibration of the strain gages, COD gages and the load cell was completed just prior to initiation of the tensile load which was applied at a rate of 11 to 25 kN/s until fracture occurred. Two exceptions to this procedure occurred during this series of tests. Specimen WP-1.1 was initially warm prestressed to guard against initiation at a low load, and specimen WP-1.4 utilized a pillow jack device to initiate crack propagation at a prescribed tensile load.

4. TEST SUMMARY

4.1 WP-1 Test Series

Table 3 presents a summary of conditions for each test in the WP-1 test series. Descriptions of tests WP-1.1 through WP-1.7 have been presented previously in Refs. [3] and [4]. Only a summary of test WP-1.7 will be provided below. However, the transverse temperature profiles at the approximate time of crack-initiation for all the tests are summarized in Fig. 4, while the fracture surfaces for specimens WP-1.1 through WP-1.6 are presented in Fig. 5, and Fig. 6 presents the fracture surface for specimen WP-1.7. These fracture surfaces show evidence of the important observation that arrest of the cleavage propagations occurred in each test prior to initiation of ductile fracture. All strain gage and acoustic emission data verify this behavior. Some of these arrests occurred at temperatures well above that which corresponds to the onset of Charpy upper-shelf behavior.

Test WP-1.7 was the seventh test in the WP-1 series and the first which utilized a 152-mm-thick specimen. After obtaining a satisfactory thermal gradient, Fig. 4, the specimen was loaded at an average rate of 17 kN/s until the testing machine's tensile load capacity, 26.7 MN, was

Table 3. Summary of HSST wide-plate crack-arrest test conditions for WP-1 series

Test No.	Crack location (cm)	Crack temperature (°C)	Initiation load (MN)	Arrest location (cm)	Arrest temperature (°C)	Arrest $T - RT_{NDT}$ (°C)
WP-1.1[a]	20	-60	20.1	50.2	51	74
WP-1.2A	20	-33	18.9	55.5	62	85
WP-1.2B	55.5	62	18.9	64.5	92	115
WP-1.3	20[b]	-51	11.25	48.5	54	77
WP-1.4A	20.7[b,c]	-63	7.95	44.1	29	52
WP-1.4B	44.1	29	9.72	52.7	60	83
WP-1.5A	20[b]	-30	11.03	52.1	56	79
WP-1.5B	52.1	56	11.03	58.0	72	95
WP-1.6A	20[b]	-19	14.50	49.3	54	77
WP-1.6B	49.3	54	14.50	59.3	80	103
WP-1.7A	20.2[b]	-24	26.2	52.8	61	84
WP-1.7B	52.8	61	26.2	63.5	88	111

[a] Specimen was warm prestressed by loading to 10 MN at 70°C. Specimen was also preloaded to 19 MN.

[b] Crack front cut to chevron configuration.

[c] Pillow jack utilized to apply pressure load to specimen's machined notch.

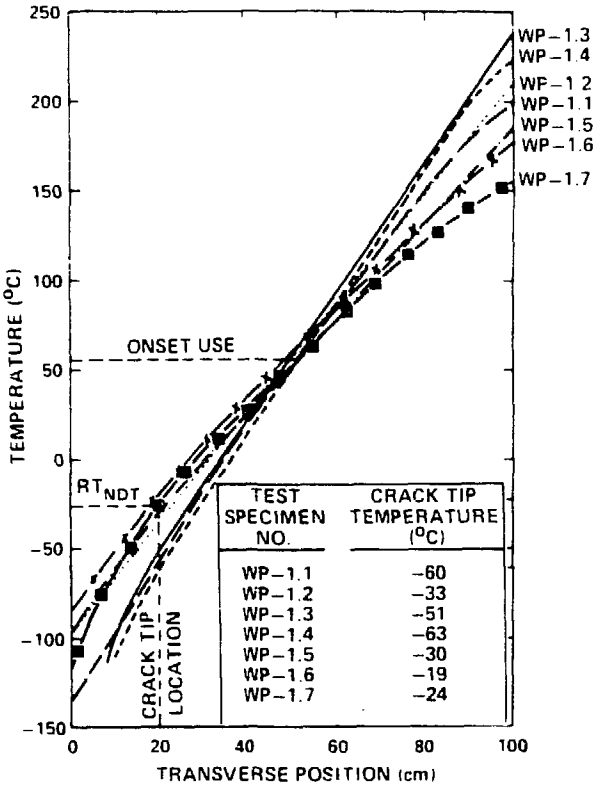

Fig. 4. Transverse temperature profile at approximate time of crack initiation-arrest events: WP-1 series.

reached. A crack run-arrest event had not occurred so the load was held constant for 176 s to see if a crack run-arrest event would initiate. Since a crack run-arrest event did not occur during this constant load period, the specimen was rapidly unloaded in an effort to sharpen the crack tip prior to application of a second load cycle. Two changes were then made in the testing procedure prior to application of a second load cycle: the crack tip temperature was lowered by about 5°C to -23.7°C, and the specimen loading rate was increased by a factor of five. Approximately 4700 s after the beginning of the first load cycle, specimen loading was reinitiated at a rate of 90 kN/s. At a load of 26.2 MN, the crack run-arrest events initiated and lasted approximately 27.5 ms (crack run-arrest events plus ductile tearing). Examination of the fracture surface (Fig. 6) indicated that two cleavage crack run-arrest events occurred. The first event lasted about 0.7 ms, with the second occurring about 7 ms after completion of the first event.

4.2 WP-2 Test Series

Table 4 presents a summary of conditions for each test in the WP-2 test series. Descriptions of tests WP-2.4 and WP-2.1 were presented in Ref. [3], while WP-2.3 and WP-2.5 were described in Ref. [4]. Only a summary of test WP-2.5 will be provided here. Transverse temperature profiles

Fig. 5. Fracture surfaces of specimens WP-1.1 through WP-1.6.

Fig. 6. Fracture surface of 152-mm-thick specimen WP-1.7.

Table 4. Summary of HSST wide-plate crack-arrest test conditions for WP-2 series

Test No.	Crack location (cm)	Crack temperature (°C)	Initiation load (MN)	Arrest location (cm)	Arrest temperature (°C)	Arrest $T - RT_{NDT}$ (°C)
WP-2.4A[a]	20.3	45	7.52	25.1	61	1
WP-2.4B	25.1[b]	61	8.85	33.8	86	26
WP-2.4C	33.8	86	8.85	39.7	102	42
WP-2.4D	39.7	102	8.85	41.3	107	47
WP-2.4E	41.3	107	8.85	46.2	121	61
WP-2.4F	46.2	121	8.85	48.4	127	67
WP-2.4G	48.4	127	8.85	51.5	137	77
WP-2.4H	51.5	137	8.85	55.5	149	89
WP-2.1A[a]	19.9	55	11.90	27.5	80	20
WP-2.1B	27.5	80	11.90	33.5	96	36
WP-2.1D	33.5	96	11.90	37.0	105	45
WP-2.1E	37.0	105	11.90	40.0	112	52
WP-2.1F	40.0	112	11.90	45.0	125	65
WP-2.1H	45.0	125	11.90	49.0	135	75
WP-2.1I	49.0	135	11.90	52.7	145	85
WP-2.1J	52.7	145	11.90	55.5	152	92
WP-2.5A[a]	19.9	66	7.53	27.2	86	26
WP-2.5B	27.2[b]	86	8.90	35.0	104	44
WP-2.5C	35.0	104	8.90	43.5	124	64
WP-2.5D	43.5	124	8.90	47.8	135	75
WP-2.5E	47.8	135	8.90	51.6	144	84
WP-2.5F	51.6	144	8.90	56.0	154	94
WP-2.3A	20.0	66	15.3	34.0	97	37
WP-2.3B	34.0	97	15.3	37.5	106	46
WP-2.3D	37.5	106	15.3	39.7	111	51
WP-2.3F	39.7	111	15.3	45.7	126	66

[a]Crack front cut to chevron configuration.

[b]After pop-in.

at the approximate time of crack-initiation events for all the tests are summarized in Fig. 7. The fracture surfaces for the four specimens in the WP-2 series tested to date are presented in Fig. 8.

Test WP-2.5 was the third utilizing the low-upper-shelf base material. After achieving the desired thermal gradient, Fig. 7, specimen loading was initiated at an average rate of 25 kN/s. At 7.53 MN, or 86% of peak load, a pop-in was heard, which was later supported by the strain gage outputs, accelerometer readings and examination of the fracture surface. Specimen loading was continued, and at a load of 8.9 MN, the fracture event began and lasted about 90 ms (cleavage fracture plus ductile tearing). Examination of the strain-gage output and fracture surface revealed that six cleavage crack run-arrest events occurred prior to the onset of ductile tearing. The entire set of cleavage run-arrest

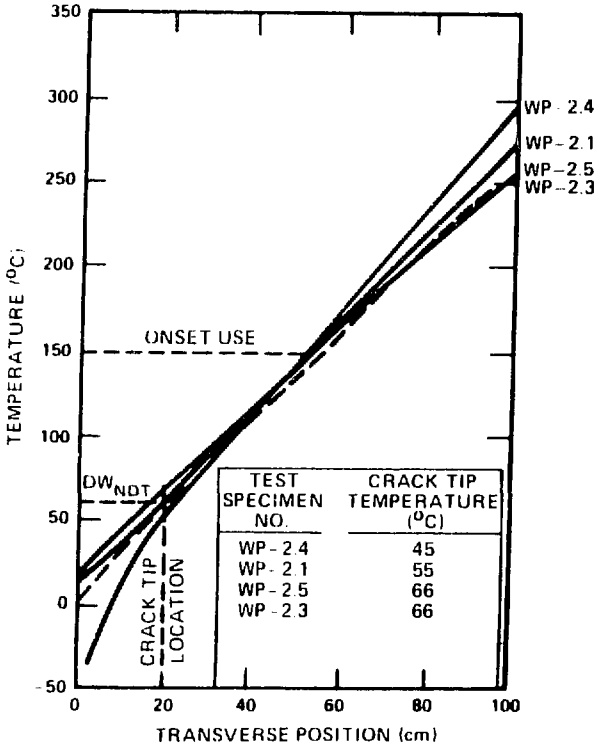

Fig. 7. Transverse temperature profile at approximate time of crack initiation-arrest events: WP-2 series.

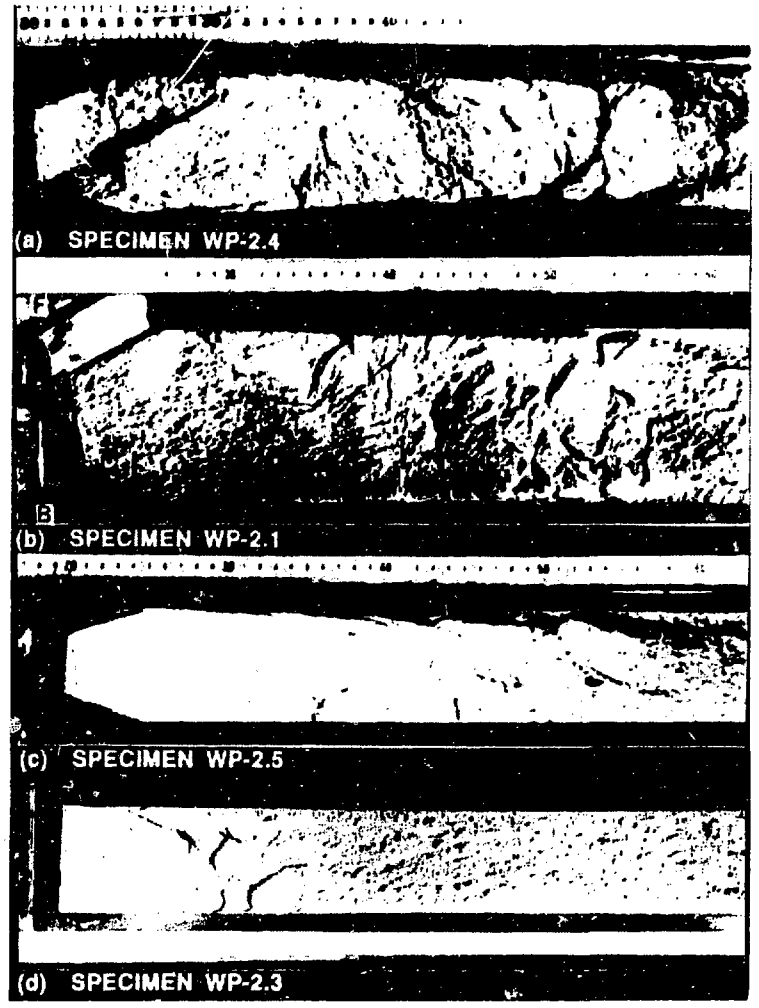

Fig. 8. Fracture surfaces of specimens WP-2.4, -2.1, -2.5 and -2.3.

events occurred over a 40 ms time span. As with the WP-1 material, arrest of cleavage propagation preceded the occurrence of ductile tearing or failure due to tensile instability (see Fig. 8).

5. POSTTEST ANALYSES AND COMPARISON WITH OTHER LARGE-SCALE TEST RESULTS

Posttest analyses were conducted for each wide-plate crack-arrest test to investigate the interaction of parameters (plate geometry, material properties, temperature profile and mechanical loading) that affect the crack run arrest events. Three-dimensional (3-D), static, finite-element analyses were performed to determine the stress-intensity factor at the time of crack initiation using the ORMGEN/ORVIRT [5,6] fracture analysis system in conjunction with the ADINA-84 [7] finite-element code. Quasistatic analyses utilized the ORNL computer code WPSTAT [8] to evaluate the static stress-intensity factors as a function of crack length and temperature differential across the plate. WPSTAT also categorizes arrested crack lengths in terms of three types of instability limits; i.e., reinitiation, tearing instability and tensile instability. Elastodynamic analyses are carried out using the ADINA/VPF [7,9] dynamic crack analysis code. The code is capable of performing both application-mode (crack tip is propagated incrementally when K_I, the dynamically computed stress-intensity factor, equals the specified dynamic fracture toughness value, K_{ID}) and generation-mode (crack tip is propagated incrementally according to a prescribed crack position vs time relationship with the values of fracture toughness determined from the dynamically computed K_I) analyses. For both modes of analysis, the dynamic stress-intensity factor is determined in each time step from the dynamic J-integral containing the appropriate inertial and thermal terms.

Table 5 summarizes crack-arrest toughness values for the WP-1 series which were computed by both static and dynamic analyses as well as those determined using handbook techniques [10,11]. The results for the WP-1 series exhibit a significant increase in toughness at temperatures near and above the onset of Charpy upper shelf ($T - RT_{NDT} = 78°C$). Crack-arrest toughness values obtained from this series of tests extend consistently above the ASME reference fracture-toughness curve. The increase in arrest-toughness values which occurs at an accelerating rate with temperature near and above the onset of Charpy upper shelf suggests that a temperature limit exists at or below which cleavage crack propagation will arrest, no matter how high the applied driving force. Figure 9 shows the initiation and arrest temperatures for the cleavage crack propagation events in the WP-1 tests, and illustrates that arrests did occur at temperatures above the onset of Charpy upper shelf.

Table 6 summarizes crack-arrest toughness values for the WP-2 test series computed using both static and dynamic analyses as well as those determined using handbook techniques. The importance of the analysis method (static vs dynamic) and boundary conditions (fixed load or fixed load-pin displacement) utilized to interpret the wide-plate crack-arrest tests is demonstrated by comparing the values listed in Table 6 for

Table 5. Summary of crack-arrest toughness values for the WP-1 test series

Test No.	Crack-arrest toughness values ($MPa\sqrt{m}$)			
	Tada static SEN formulas		Fedderson alternate secant formula[c]	Dynamic FE[d]
	Displ. control[a]	Load control[b]		Generation mode
WP-1.1	391	813	340	NA
WP-1.2A	384	942	349	424
WP-1.2B	416	1489	419	685
WP-1.3	215	424	185	235
WP-1.4A	145	248	120	NA
WP-1.4B	331	433	170	387
WP-1.5A	217	472	191	231
WP-1.5B	229	616	213	509
WP-1.6A	279	565	242	275
WP-1.6B	306	881	290	397
WP-1.7A	351	793	311	319
WP-1.7B	385	1312	381	555

[a] From Ref. [10] (pp. 2.10-2.11) while assuming $a = a_f$ and no further bending occurs due to propagation of the crack.

[b] From Ref. [10] (pp. 2.10-2.11) while assuming $a = a_f$ and full bending according to SEN formula when the final crack depth is used.

[c] $K_I = \sigma \left\{ \pi a \sec\left(\frac{\pi a}{2w}\right) \right\}^{1/2}$ with σ = far-field tensile stress, $a = a_f$ = final crack length, and w = full plate width (Ref. [11]).

[d] Dynamic finite element analyses (fixed load) using ORNL program ADINA/VPF (Refs. [7,9]).

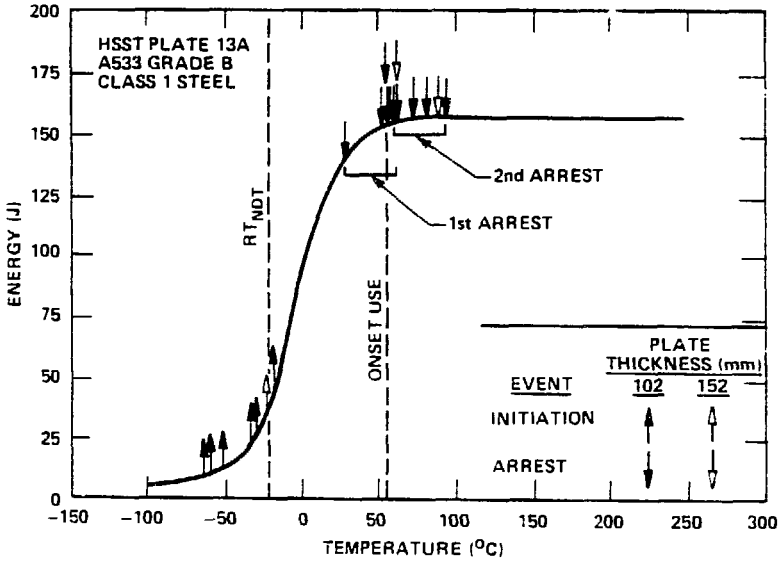

Fig. 9. Charpy V-notch energy versus temperature and cleavage arrest temperatures for the WP-1 series test specimens.

Table 6. Summary of crack-arrest toughness values for the WP-2 test series

Test No.	Crack-arrest toughness values ($MPa\cdot\sqrt{m}$)			
	Tada static SEN formulas		Fedderson alternate secant formula [c]	Dynamic FE [d]
	Displ. control [a]	Load control [b]		Generation mode
WP-2.4A	104	113	79	---
WP-2.4B	155	186	111	137
WP-2.4C	168	234	124	188
WP-2.4D	171	249	128	281
WP-2.4E	181	303	140	249
WP-2.4F	185	332	145	307
WP-2.4G	191	378	153	381
WP-2.4H	198	451	165	397
WP-2.1A	114	132	88	106
WP-2.1B	126	166	100	153
WP-2.1D	133	190	106	158
WP-2.1E	138	213	112	170
WP-2.1F	146	260	123	201
WP-2.1H	153	306	132	293
WP-2.1I	158	359	141	371
WP-2.1J	163	406	149	406
WP-2.5A	108	123	83	---
WP-2.5B	165	196	114	171
WP-2.5C	184	273	134	190
WP-2.5D	193	326	144	268
WP-2.5E	200	382	155	306
WP-2.5F	209	464	167	366
WP-2.3A	164	217	129	144
WP-2.3B	172	249	138	232
WP-2.3D	177	271	144	255
WP-2.3F	190	344	160	258

[a] From Ref. [10] (pp. 2.10–2.11) while assuming $a = a_f$ and no further bending occurs due to propagation of the crack.

[b] From Ref. [10] (pp. 2.10–2.11) while assuming $a = a_f$ and full bending according to SEN formula when the final crack depth is used.

[c] $K_I = \sigma \left\{ \pi a \sec\left(\frac{\pi a}{2w}\right) \right\}^{1/2}$ with σ = far-field tensile stress, $a = a_f$ = final crack length, and w = full plate width (Ref. [11]).

[d] Dynamic finite element analyses (fixed load) using ORNL program ADINA/VPF (Ref. [7,9]).

specimen WP-2.4. Values of K_{Ia} determined using the secant equation [11] and the Tada fixed-load condition [10] represent approximate lower and upper bounds, respectively, to the results, Fig. 10. For the long-durations of the crack run-arrest events (>20 ms) observed for the LUS WP-2 material, considerable load adjustment can take place as a result of specimen/pull-plate compliance. Therefore, the most meaningful calculations of K_{Ia} values under such conditions must take these factors into account through the use of a dynamic finite-element analysis. For example, dynamic generation-mode (fixed load and fixed displacement) analysis results for test WP-2.4 are also shown in Fig. 10. Note that the long fracture durations lead to dynamic results that appraoch those predicted by load-controlled static calculations. Figure 11 presents the fixed-load, generation-mode dynamic finite-element determinations of K_{Ia} for all the WP-2 series tests conducted to date, and illustrates a consistent trend to high toughness conditions.

5.2 Comparison of Data with Other Large-Scale Test Results

Results presented in Fig. 11 show that the wide-plate K_{Ia} test results for WP-2 exhibit an accelerating increase in arrest-toughness values with increasing temperature. This trend for K_{Ia} values extends consistently well above the limit provided in ASME Section XI. This trend combines well with that for WP-1 material when K_{Ia} is plotted against $T - RT_{NDT}$ as illustrated in Fig. 12. Figure 12 also presents data from several other types of large-scale tests [12-16] that show very reasonable agreement even when the RT_{NDT} values differ by more than 120°C.

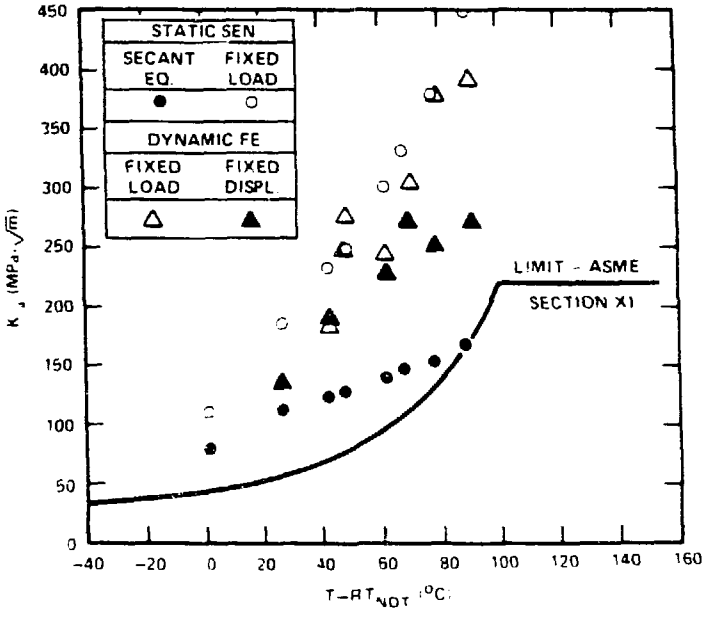

Fig. 10. Static and dynamic crack-arrest toughness determination versus temperature ($T - RT_{NDT}$) for specimen WP-2.4.

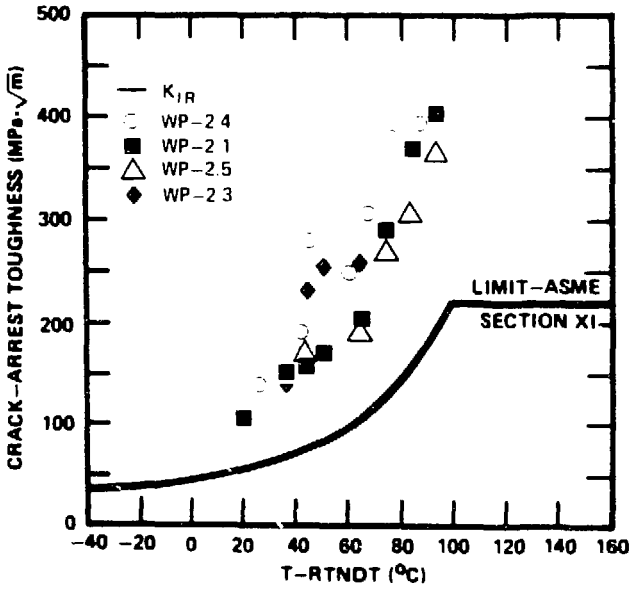

Fig. 11. Fixed-load generation mode crack-arrest toughness data versus temperature (T - RT_{NDT}) for test series WP-2.

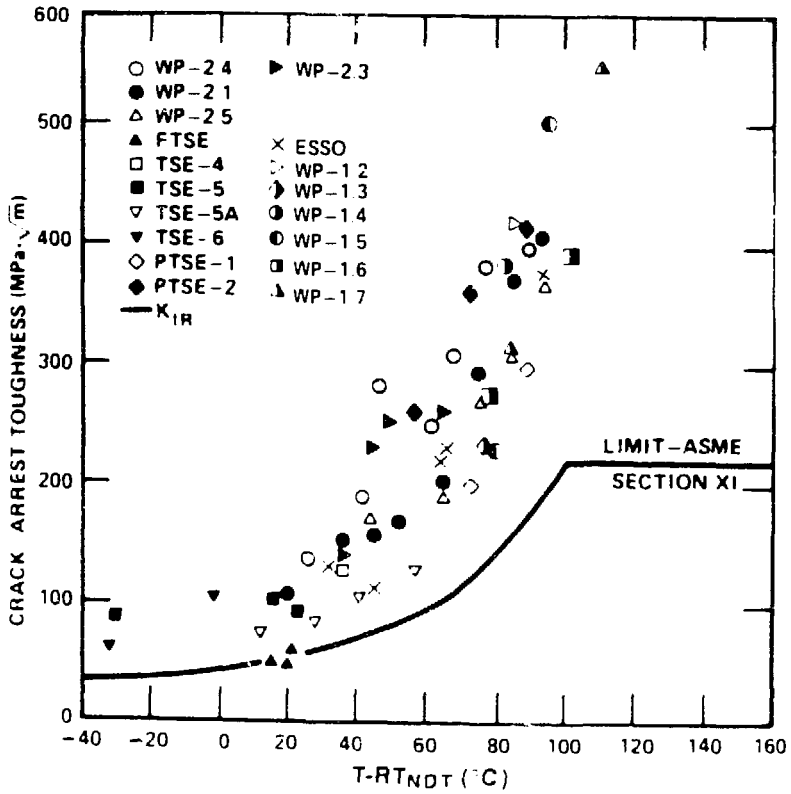

Fig. 12. High-temperature crack-arrest toughness data versus temperature (T - RT_{NDT}) for wide-plate and large specimen tests.

6. VISCOPLASTIC DYNAMIC FRACTURE ANALYSIS METHODS

6.1 Motivation for Inelastic Methods Development

Until recently, linear elastic fracture mechanics (LEFM) concepts have been dominant in applications of dynamic analysis techniques to the crack-arrest studies described in the previous sections. The basic postulate of LEFM requires that the inelastic deformation surrounding the crack tip be contained within the K_I-dominant region. The K_I-dominant region represents a sufficiently small neighborhood of the crack-tip where loading conditions and specimen geometry affect the strength of the elastic fields only through the stress-intensity factor K_I. Furthermore, it is assumed that rapid crack propagation is governed by a unique geometry-independent material property, the dynamic fracture toughness K_{ID} [for example, see Eq. (4)]. Propagation of a running crack occurs under the condition that the applied dynamic stress-intensity factor K_I satisfies the relation

$$K_I = K_{ID}(\dot{a},T) \tag{9}$$

where K_{ID} is taken to be a function of the crack-tip velocity, $\dot{a}$, and the temperature, T. However, except for very short crack jumps, LEFM assumptions are not strictly valid characterizations of rapid crack propagation [17]. In particular, a wake of residual plasticity left behind the moving crack tip violates the K_I-dominance requirement of LEFM. An indication that LEFM conditions are not satisfied occurs when elastodynamic analyses of crack run-arrest data lead to geometry-dependent fracture toughness relations. Dahlberg, et al. [18] performed elastodynamic fracture analyses using crack run-arrest data from tests of single-edge-notched (SEN) tension panel specimens of different lengths. The material employed in their experiments was a strain-rate dependent high-strength carbon steel. As shown in Fig. 13, their results for different panel lengths coincide for low crack velocities, but show a definite geometry dependence at higher velocities where nonlinear effects are more pronounced. However, Brickstad [19] has demonstrated that this geometry dependence can be removed through application of an inelastic fracture model that incorporates plasticity and strain-rate effects (i.e., viscoplasticity). Brickstad's results obtained by applying the viscoplastic model of Perzyna [20] to the experimental data of Ref. 18 are also shown in Fig. 13.

In general, viscoplastic (or unified) constitutive theories attempt to represent various manifestations of time-dependent inelastic behavior, such as creep, stress relaxation, and plastic flow, by a single kinematic equation and discrete set of state variables. The motivation for developing such theories has, over the last 15 years, come mostly from interest in high-temperature applications. There high temperature is taken to be in the range where observable creep deformations occur over long periods of time when the stress levels are near the engineering yield stress. However, rate effects can also be very important for rapid-loading situations such as the rapid crack propagation events in

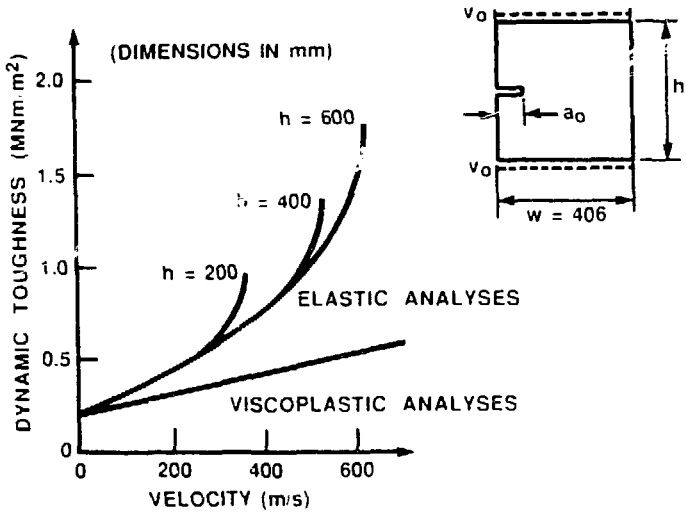

Fig. 13. Dynamic fracture toughness relations determined for SEN tension panel specimens of different lengths (from Refs. 18 and 19).

ductile structural alloys, where the temperature for transition from brittle to ductile fracture may be well below the classical creep regime. These events are accompanied by high strain rates ($\sim 10^4$ s^{-1}) in the vicinity of a fast-running crack. The role of viscoplasticity in the prediction of run-arrest behavior in these ductile steels has been examined by several recent studies [19,21] which emphasized the importance of including viscoplastic effects in constitutive relations. The HSST program is supporting research efforts at ORNL and several subcontracting groups to develop viscoplastic dynamic finite element analysis techniques and to validate their utility through analyses of carefully controlled experiments. These analysis capabilities are expected to give an improved basis for establishing and unifying appropriate fracture criteria that govern dynamic crack propagation-arrest behavior in RPV steels.

As part of this development, various viscoplastic constitutive models and several proposed nonlinear fracture criteria have been installed in general purpose (ADINA/VPF) [7,9] and special purpose (VISCRK) [22] finite element computer programs. The constitutive models implemented in these computer programs include the Bodner-Partom [23] and the Perzyna [20] viscoplastic formulations; the proposed fracture criteria include three parameters (T* from Ref. 24, J from Ref. 25, and γ from Ref. 19) that are based on energy principles. Dynamic stress-strain data from tensile and split-Hopkinson bar tests have been used to derive constants for the Bodner-Partom and the Perzyna models appropriate for A533 grade B class 1 steel [26].

6.2 Applications to Wide-Plate Tests

The predictive capabilities of these nonlinear techniques are being evaluated through applications to the series of HSST wide-plate crack-

arrest tests. As an example, results from viscoplastic dynamic analyses of one wide-plate test (WP-1.2) utilizing the Bodner-Partom constitutive model are shown in Fig. 14. Generation-mode fixed load dynamic analyses [27] of WP-1.2 were performed using the ADINA/VPF code [7,9] and the estimate of crack position versus time is given in Fig. 14(a). The time histories of parameters T*, J, and γ are expressed in terms of pseudo-K_I values for purposes of comparison with elastodynamic values shown in Fig. 14(b). The results in Fig. 14 indicate good agreement between the functions for both elastic and inelastic analyses and demonstrate the significance of including viscoplasticity in the fracture parameter calculations. Dissipative processes that occur in the developing plastic

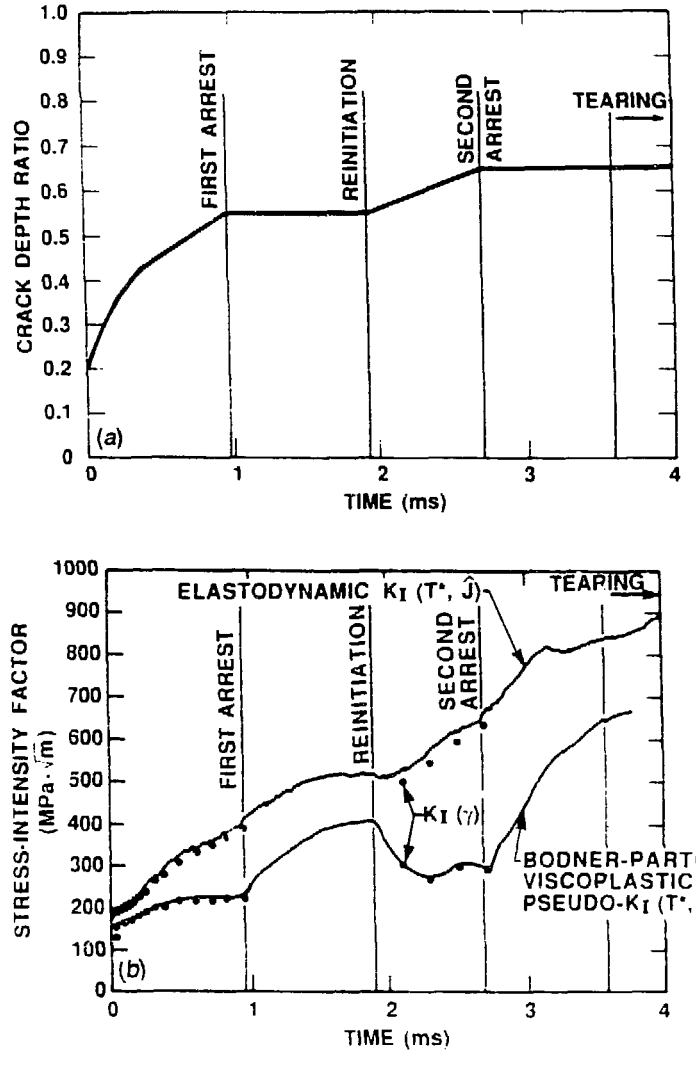

Fig. 14. Crack-depth ratio and amplitude of stress-intensity-factor versus time in generation-mode elastodynamic and viscoplastic dynamic analyses of wide-plate test WP-1.2: (a) crack-depth ratio versus time; and (b) amplitude of stress-intensity factor versus time.

zone lead to reduced energy flow to the crack-tip region and, hence, to lower values for the fracture parameters (compared to elastodynamic values). However, a more definitive evaluation of the utility of these fracture parameters in predicting crack run-arrest behavior in wide plates must await results from further numerical studies. Results in Fig. 15 obtained from models having different mesh refinements along the crack plane indicate that the viscoplastic dynamic solutions of the wide-plate tests have not yet converged for the mesh refinements employed thus far. It has not yet been established what degree of mesh refinement is necessary to get convergence of the fracture parameters, or whether the parameters will converge to non-zero values.

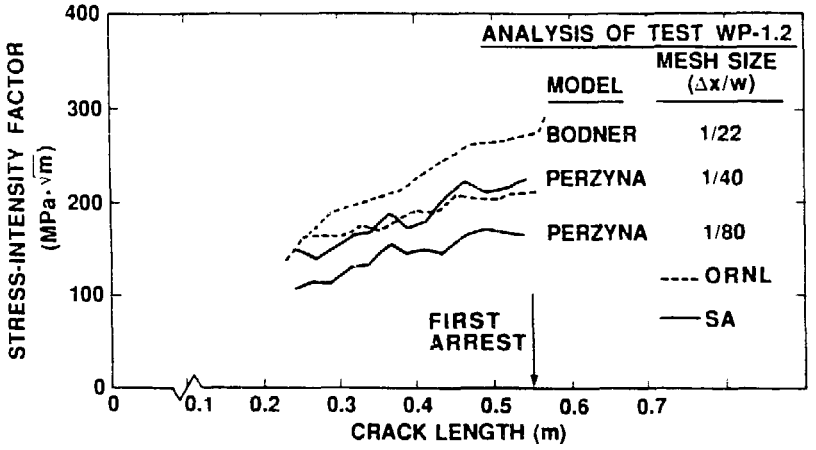

Fig. 15. Comparison of results [$K_I(\gamma)$ vs crack depth] from generation-mode viscoplastic dynamic analyses of test WP-1.2 for three crack path mesh refinements.

7. CONCLUSIONS

In conclusion, the HSST program has an integrated effort under way to extend the range of applicability of current state-of-the-art crack-arrest practices and to develop alternatives where improvements are needed. Fractographic examinations confirm that the crack propagation in the wide-plate tests occurred by a predominately cleavage mode and that the arrest events were not preceded by conversion to ductile tearing. Arrest may be followed by stable or unstable ductile crack growth, but these modes of fracture may be analyzed independent of the cleavage run-arrest events. A consistent trend is formed when the crack-arrest data from the various types of HSST large-specimen tests are combined on a plot of K_{Ia} vs $T - RT_{NDT}$ with data from large-specimen tests at other laboratories. Dynamic effects must be included in the analysis techniques to obtain meaningful calculations for the relatively thin plate-type specimens. Collectively these data show that cleavage propagation can occur at temperatures up to and above that which corresponds to the onset of Charpy upper-shelf behavior, and the measured K_{Ia} values extend

well above the limit included in Section XI of the ASME code. Further, the data suggest the existence of a limiting temperature above which a cleavage crack cannot propagate no matter how high the applied driving force.

The role of nonlinear rate-dependent effects in the interpretation of crack run-arrest events in these ductile materials is being investigated through development and applications of viscoplastic dynamic finite element analysis techniques. Comparisons of elastodynamic and viscoplastic dynamic fracture analyses of tests from the WP-1 series indicate that the effects of including viscoplasticity in the fracture parameter calculations are significant for certain crack run-arrest events. Future development plans include mesh refinement studies to determine whether the proposed fracture parameters converge to non-zero values in viscoplastic analyses on whether they are controlled by the element length used along the path of crack propagation. Planned applications of alternative crack-modeling techniques, such as moving variable-order singular elements, will possibly lead to better resolution of stress and strain fields ahead of the propagating crack and thus to improved understanding of the significance of the proposed fracture criteria.

REFERENCES

1. M. F. Kanninen et al., *Preliminary Analysis of Japanese Wide-Plate Dynamic Crack Propagation Arrest Experiments*, Subcontract report from Battelle Columbus Laboratories to Oak Ridge National Laboratory, December 1983.

2. G. A. Danko et al., *Wide-Plate Crack-Arrest Tests: Instrumentation for Dynamic Strain Measurements*, NBSIR 85-3289, National Bureau of Standards, Gaithersburg, Maryland, December 1985.

3. C. E. Pugh and D. J. Naus, "Integration of Wide-Plate Crack-Arrest Test Results," *Proc. of U.S. Nuclear Regulatory Commission Fourteenth Water Reactor Safety Information Meeting* held at National Bureau of Standards, Gaithersburg, Maryland, NUREG/CP-0082, pp. 195-225, February 1987.

4. D. J. Naus, et al., "Summary of HSST Wide-Plate Crack-Arrest Tests and Analyses," *Proc. of U.S. Nuclear Regulatory Commission Fifteenth Water Reactor Safety Information Meeting held at National Bureau of Standards*, Gaithersburg, Maryland, NUREG/CP-0091, pp. 17-40, February 1988.

5. B. R. Bass and J. W. Bryson, *Applications of Energy Release Rate Technique to Part-Through Cracks in Plates and Cylinders, Volume 1, ORMGEN-3D: A Finite Element Mesh Generator for 3-Dimensional Crack Geometries*, NUREG/CR-2997, Vol. 1 (ORNL/TM-8527/V1), Union Carbide Corp. Nuclear Div., Oak Ridge Natl. Lab., December 1982.

6. B. R. Bass and J. W. Bryson, *Applications of Energy Release Rate Technique to Part-Through Cracks in Plates and Cylinders, Volume 2, ORVIRT: A Finite Element Program for Energy Release Rate Calculations for 2-D and 3-D Crack Models*, NUREG/CR-2997, Vol. 2 (ORNL/TM-8527/V2), Union Carbide Corp., Nuclear Div., Oak Ridge Natl. Lab., February 1983.

7. K. J. Bathe, *ADINA - A Finite Element Program for Automatic Dynamic Incremental Nonlinear Analyses*, Report A-1, Massachusetts Institute of Technology, Cambridge, Mass., 1984.

8. B. R. Bass, C. E. Pugh, and H. K. Stamm, "Dynamic Analyses of a Crack Run-Arrest Experiment in a Nonisothermal Plate," *Pressure Vessel Components Design and Analysis*, ASME Publication PVP, 98-2, 175-84, 1985.

9. B. R. Bass and J. Keeney-Walker, "Computer Program Development for Dynamic Fracture Analysis," pp. 5-12 in *Heavy-Section Steel Technology Program Semiann. Prog. Rep. April-September 1985*, NUREG/CR-4219, Vol. 2 (ORNL/TM-9593/V2), Martin Marietta Energy Systems, Inc., Oak Ridge Natl. Lab., January 1986.

10. R. Tada, P. C. Paris, and G. R. Irwin, *The Stress Analysis of Cracks Handbook*, Del Research Corp., Hellertown, Pa., 1973.

11. C. F. Fedderson, *Current Status of Plane Strain Crack Toughness Testing of High-Strength Metallic Materials*, Crack Arrest Methodology and Applications, ASTM STP-410, American Society for Testing and Materials, Philadelphia, Pa., 1967.

12. R. D. Cheverton et al., "Fracture Mechanics Data Deduced from Thermal-Shock and Related Experiments with LWR Pressure Vessel Material," *J. Pressure Vessel Technol.* 105, 102-10 (May 1983).

13. R. H. Bryan et al., *Pressurized-Thermal-Shock Test of 6-in.-Thick Pressure Vessels. PTSE-1: Investigation of Warm Prestressing and Upper-Shelf Arrest*, NUREG/CR-4106 (ORNL-6135), Martin Marietta Energy Systems, Inc., Oak Ridge Natl. Lab., April 1985.

14. Japan Welding Council, *Structural Integrity of Very Thick Steel Plate for Nuclear Reactor Pressure Vessels*, JWES-AE-7806, Tokyo, 1977 (in Japanese).

15. A. Pellissier-Tanon, P. Sollogoub, and B. Houssin, "Crack Initiation and Arrest in an SA 508 Class-3 Cylinder Under Liquid Nitrogen Thermal-Shock Experiment," *Transactions of the 7th International Conference on Structural Mechanics in Reactor Technology*, Chicago, Vols. G and H, 132-42 (August 1983).

16. R. H. Bryan et al., *Quick-Look Report on the Second HSST Pressurized-Thermal-Shock Test, PTSE-2*, ORNL/PTSE-2, Martin Marietta Energy Systems, Inc., Oak Ridge Natl. Lab., February 19, 1987.

17. M. F. Kanninen and C. H. Popelar, *Advanced Fracture Mechanics*, Oxford University Press, New York, 1985, pp. 214—230.

18. L. Dahlberg et al., "Influence of Specimen Geometry on Crack Propagation and Arrest Toughness," *Crack Arrest Methodology and Applications*, ASTM STP-711, American Society for Testing and Materials, Philadelphia, Pa., G. T. Hahn and M. F. Kanninen (Eds), pp. 89—108 (1980).

19. B. Brickstad, "A Viscoplastic Analysis of Rapid Crack Propagation Experiements in Steel," *J. Mech. Phys. Solids*, Vol. 31, pp. 307-327 (1983).

20. P. Perzyna, "Fundamental Problems in Visco-Plasticity," pp. 244-368 in *Recent Advances in Applied Mechanics*, Academic Press, New York, 1966.

21. R. Hoff, C. A. Rubin, and G. T. Hahn, *Strain-Rate Dependence of the Deformation at the Tip of a Stationary Crack*, ASTM STP-868, American Society for Testing and Materials, Philadelphia, Pa., pp. 409—430 (1985).

22. R. J. Dexter et al., "Dynamic-Viscoplastic Analysis and Small-Specimen Experimental Methods for the Study of Fracture in A533B Steel," in *Proceedings of the Fourth International Conference on Numerical Methods in Fracture Mechanics, March 23—27, 1987, San Antonio, TX.*

23. S. R. Bodner and Y. Partom, "Constitutive Equations for Elastic Viscoplastic Strain Hardening Materials," *J. Appl. Mech.*, Vol. 42, p. 385 (1975).

24. S. N. Atluri, T. Nishioka, and M. Nakagaki, "Incremental Path Independent Integrals in Inelastic and Dynamic Fracture Mechanics," *Eng. Fract. Mech.* Vol. 20-2, pp. 209—244 (1984).

25. K. Kishimoto, S. Aoki, and M. Sakata, "On the Path-Independent Integral — J," *Eng. Fract. Mech.*, Vol. 13, pp. 841—50 (1980).

26. M. F. Kanninen et al., "Viscoplastic Characterization of A533B Steel," in *Heavy-Section Steel Technology Program Semiann. Prog. Rep. April— September 1986*, NUREG/CR-4219, Vol. 3, No. 2 (ORNL/TM-9593/V3&N2), Martin Marietta Energy Systems, Inc., Oak Ridge Natl. Lab., Dec. 1986.

27. B. R. Bass et al., "Evaluation of Viscoplastic Fracture Criteria and Analysis Methods," *Proc. of U.S. Nuclear Regulatory Commission Fifteenth Water Reactor Safety Information Meeting*, National Bureau of Standards, Gaithersburg, Maryland, NUREG/CP-0091, pp. 59—91, February 1988.

END

DATE FILMED

01 / 21 / 88